Insights into Interfacial Synergistic Catalysis over Ni@TiO$_{2−x}$ Catalyst toward Water−Gas Shift Reaction

Ming Xu,[†] Siyu Yao,[‡] Deming Rao,[†] Yiming Niu,[§] Ning Liu,[†] Mi Peng,[‡] Peng Zhai,[‡] Yi Man,[∥] Lirong Zheng,[⊥] Bin Wang,*,[∥] Bingsen Zhang,*,[§] Ding Ma,*,[‡] and Min Wei*,[†]

[†]State Key Laboratory of Chemical Resource Engineering, Beijing Advanced Innovation Center for Soft Matter Science and Engineering, Beijing University of Chemical Technology, Beijing 100029, People's Republic of China

[‡]College of Chemistry and Molecular Engineering and College of Engineering, BIC-ESAT, Peking University, Beijing 100871, People's Republic of China

[§]Shenyang National Laboratory for Materials Science, Institute of Metal Research, Chinese Academy of Sciences, Shenyang 110016, People's Republic of China

[∥]Beijing Research Institute of Chemical Industry, Sinopec Group, Beijing 100013, People's Republic of China

[⊥]Institute of High Energy Physics, the Chinese Academy of Sciences, Beijing 100049, People's Republic of China

Ⓢ *Supporting Information*

ABSTRACT: The mechanism on interfacial synergistic catalysis for supported metal catalysts has long been explored and investigated in several important heterogeneous catalytic processes (e.g., water−gas shift (WGS) reaction). The modulation of metal−support interactions imposes a substantial influence on activity and selectivity of catalytic reaction, as a result of the geometric/electronic structure of interfacial sites. Although great efforts have validated the key role of interfacial sites in WGS over metal catalysts supported on reducible oxides, direct evidence at the atomic level is lacking and the mechanism of interfacial synergistic catalysis is still ambiguous. Herein, Ni nanoparticles supported on TiO$_{2−x}$ (denoted as Ni@TiO$_{2−x}$) were fabricated via a structure topotactic transformation of NiTi-layered double hydroxide (NiTi-LDHs) precursor, which showed excellent catalytic performance for WGS reaction. *In situ* microscopy was carried out to reveal the partially encapsulated structure of Ni@TiO$_{2−x}$ catalyst. A combination study including *in situ* and *operando* EXAFS, *in situ* DRIFTS spectra combined with TPSR measurements substantiates a new redox mechanism based on interfacial synergistic catalysis. Notably, interfacial Ni species (electron-enriched Ni$^{\delta−}$ site) participates in the dissociation of H$_2$O molecule to generate H$_2$, accompanied by the oxidation of Ni$^{\delta−}$−O$_v$−Ti^{3+} (O$_v$: oxygen vacancy) to Ni$^{\delta+}$−O−Ti^{4+} structure. Density functional theory calculations further verify that the interfacial sites of Ni@TiO$_{2−x}$ catalyst serve as the optimal active site with the lowest activation energy barrier (∼0.35 eV) for water dissociation. This work provides a fundamental understanding on interfacial synergistic catalysis toward WGS reaction, which is constructive for the rational design and fabrication of high activity heterogeneous catalysts.

Interfacial synergistic catalysis
Oxygen Vacancy
CO + H$_2$O
Redox mechanism
CO$_2$ + H$_2$
● Ni ● O ● Ti
● C ● O ● H

1. INTRODUCTION

Reducible oxide supported transition metal catalysts have attracted extensive attention in many important heterogeneous catalytic reactions.[1−4] For instance, the water−gas shift reaction (WGS: CO + H$_2$O↔CO$_2$ + H$_2$), is an indispensable step in many important industrial processes and has potential applications in fuel cells. Its primary purpose is to eliminate deleterious CO present in feed streams for hydrogen production.[5] Great efforts have been devoted to studying the intrinsic active site and reaction mechanism of WGS, so as to boost the rational design of highly active heterogeneous catalysts.[6−8] However, there are still many controversies about the nature of active sites: metal site, oxide support, or metal-oxide interface. The reaction mechanism is also ambiguous.[9−12] So far, a bifunctional reaction mechanism has been generally accepted: CO adsorbs on the metal site and H$_2$O undergoes activated dissociation on the oxygen vacancies of support, followed by the subsequent reaction between the CO and the dissociative species at the metal-oxide interface.[10,11] Nevertheless, this interfacial synergistic mechanism neglects the adsorption-induced interfacial reconstruction, especially for water dissociation. Therefore, how to detect and identify the geometric structure and electronic state of active sites under *in situ* and *operando* reaction conditions remains a tremendous challenge. In addition, direct evidence on active sites at the atomic level is crucial for revealing reaction mechanism and new catalyst design.

Recently, inverse oxide/metal catalysts (e.g., CeO_{2-x}/Au(111), TiO_{2-x}/Au(111), and CeO_{2-x}/Cu(111)) have been investigated as a model system to deeply understand the role of oxide and metal-oxide interface,[11,13,14] which strongly confirmed that interfacial sites act as the active site in WGS reaction and accelerate the rate-determining step (water dissociation). In the traditional view, the chemisorption of H_2O on the oxygen vacancies of support generates active surface hydroxyl or oxygen species, and admetal facilitates the dissociation of H_2O indirectly through promoting the formation of oxygen vacancies during the reduction of catalysts.[15,16] More recently, Rodriguez et al. developed a facile approach to construct $Pt/CeO_x/TiO_2(110)$ catalyst with a new type of strong metal–support interactions (SMSI), which involved electronic perturbation of small Pt particles in contact with ceria and thus significantly enhanced the cleavage of O–H bond in water.[17] Campbell et al. used density functional theory (DFT) calculations to further explore the electronic interaction between platinum and reduced ceria, and proposed a new concept of electronic metal–support interactions (EMSI) that induce a charge redistribution of the metal-oxide interface.[18] Recently, we demonstrated that $Ni@TiO_{2-x}$ catalyst with core–shell structure, which showed excellent catalytic performance for WGS reaction, has strong EMSI.[19] The phenomenon has been reported earlier by different groups that the metal–support interactions can be effectively modulated via the construction of embedded or core–shell-type catalysts[20–23] including metal supported on nonreducible oxides (e.g., $Rh@Al_2O_3$). Whereas, whether the interfacial metal sites directly participate in H_2O dissociation in the WGS reaction or not, is still unclear. Moreover, our previous study demonstrates that the strong interaction between TiO_{2-x} and Ni nanoparticles promotes the formation of abundant defect sites (O_v: oxygen vacancy and Ti^{3+} species) accompanied by the generation of interfacial $Ni^{\delta-}–O_v–Ti^{3+}$ species, which serve as dual active sites of WGS reaction.[19] Nevertheless, this was demonstrated via the quantitative relation between concentration of interfacial site ($Ni^{\delta-}–O_v–Ti^{3+}$) and the catalytic reaction rate. In situ or even operando information on catalytic mechanism is vital to a fundamental understanding on the interfacial synergistic catalysis mechanism.

Herein, we provide direct spectroscopic evidence of EMSI at the interface over $Ni@TiO_{2-x}$ catalyst and directly observe the electronic state and structural change of interfacial active sites under in situ and operando conditions. In situ HRTEM, in situ EELS combined with ex situ STEM-EDS experiments were performed to illustrate the partial encapsulation of Ni nanoparticles by TiO_{2-x} overlayer and reveal the chemical state of Ti located at the interface. A direct observation for the whole catalytic reaction process on interfacial sites was achieved by means of in situ and operando extended X-ray absorption fine structure spectroscopy (EXAFS), in situ diffuse reflectance infrared Fourier-transform spectroscopy (DRIFTS) combined with temperature-programmed surface reaction (TPSR) measurements. A redox mechanism based on interfacial synergistic catalysis was demonstrated for the first time over this type of catalyst: H_2O molecule undergoes dissociation on $Ni^{\delta-}–O_v–Ti^{3+}$ species (interfacial sites) to generate hydrogen and active oxygen species, followed by the reaction between active oxygen species and CO molecule adsorbed on the surface of Ni nanoparticles to produce CO_2. Most interestingly, through in situ EXAFS studies we can gain an insight into the electronic state, coordination environment and bond distance of Ni species during the H_2O dissociation step, which explicitly verifies that interfacial admetal directly participate in the O–H bond cleavage of water molecule, accompanied by the oxidation of $Ni^{\delta-}–O_v–Ti^{3+}$ to $Ni^{\delta+}–O–Ti^{4+}$ and concomitly the formation of hydrogen. A new interfacial synergistic catalysis was substantiated by virtue of monitoring the structural/electronic dynamic evolution of intrinsic active site and reactive species under in situ and operando conditions, which would pave the way for the rational design and development of high activity heterogeneous catalysts.

2. EXPERIMENTAL SECTION

2.1. Materials. All the chemicals ($TiCl_4$, $Ni(NO_3)_2\cdot 6H_2O$, and urea) were analytical grade, which were purchased from Sigma-Aldrich. During the whole experimental process, deionized water was used and the chemicals were used without further purification.

2.2. Preparation of $Ni@TiO_{2-x}$(450) Catalysts. The $Ni@TiO_{2-x}$(450) catalyst was synthesized according to our previous work.[19]

2.3. Catalyst Characterization. In situ HRTEM, in situ EELS and ex situ HAADF-STEM measurements: The $Ni@TiO_{2-x}$(450) catalyst was suspended in ethanol via ultrasound, and dropped onto the carbon-on-copper grids. Subsequently, the sample was installed in the nanoreactor with a heating gas holder (DENS solutions), and reduced in 10% H_2 (He, balance) at 450 °C for 1 h. Then, the obtained product was slowly cooled to ~25 °C in a He atmosphere. Subsequently, in situ HRTEM measurement was carried out on a FEI Tecnai G^2 F20 at an accelerating voltage of 200 kV. In situ electron energy loss spectroscopy (in situ EELS) was further performed to explore the encapsulation over $Ni@TiO_{2-x}$(450) sample. In situ EELS spectra were collected including the Ti L-edge spectra, O L-edge spectra and Ni L-edge spectra in various area with a spot size of ~1 nm in diameter and acquisition time of 5 s. High-angle annular dark-field scanning TEM-energy-dispersive X-ray spectroscopy (HAADF-STEM) images were obtained on a FEI Tecnai G^2 F20 instrument. In situ Ni K-edge EXAFS was carried out at the beamline 1W1B of the Beijing Synchrotron Radiation Facility (BSRF), Institute of High Energy Physics (IHEP), Chinese Academy of Sciences (CAS). The IFFEFIT package was performed for the data analysis and fitting. Before the measurement on Ni K-edge EXAFS spectra of $Ni@TiO_{2-x}$(450) sample, all the samples were prereduced in H_2 atmosphere at 450 °C for 1 h and subsequently flushed with He for 30 min. In situ DRIFTS was carried out in a reaction cell on a VERTEX 70 spectrometer, with a resolution of 4 cm^{-1}. H_2O TPD-MASS and H_2O Pulse-MASS measurements were performed on a Micromeritics ChemiSorb 2070. The temperature-programed surface reaction (TPSR) and cycling test of CO and H_2O Pulse-MASS were carried out to further explore the reaction mechanism of WGS over the $Ni@TiO_{2-x}$(450) catalyst. The detailed pretreatment conditions and test conditions are given in the Supporting Information.

2.4. DFT Calculations. DFT+U calculations were performed based on the Vienna ab-initio simulation package (VASP). A four-layer slab with $p(2\sqrt{3} \times 2\sqrt{3})$ supercell was cleaved for the surface of Ni(111),[24,25] and the model of $Ni(111)@TiO_{2-x}(101)$ was built by a free $TiO_2(101)$ single chain in a (2×1) array over the Ni(111) surface mentioned above.[11,13] The Ti center of $TiO_2(101)$ single chain over the surface was unsaturated in coordination. A four-layer slab of two repeat units with $p(3 \times 3)$ supercell was cleaved for the surface of $TiO_{2-x}(101)$,[26,27] where five-coordinated Ti center served as the active site for water dissociation. The exchange-correlation potential was described by the Perdew–Burke–Ernzerhof (PBE) generalized gradient approach (GGA).[28,29] We set the Hubbard parameters to U-J = 3 eV for Ti.[30] The DFT calculations used A $3 \times 3 \times 1$ k-point sampling in the surface Brillouin zone. The calculations of all these models considered spin polarization. The converge criteria is that the force on each relaxed atom is below 0.05 eV/ Å and an energy

cutoff is 400 eV, which were used in the calculations. The CI-NEB method was used to search transition state (TS) at the same theoretical level.[31,32] Then the calculations on adsorption energy of H_2O ($E_{ads}(H_2O)$), energy barrier of water dissociation ($\Delta E_{ads}(TS)$) and reaction heat (E_{reac}) on Ni(111), Ni(111)@TiO$_{2-x}$(101) interface, and TiO$_{2-x}$(101), were carried out.

3. RESULTS AND DISCUSSION

3.1. Structural and Morphological Characterizations of Ni@TiO$_{2-x}$(450) Sample. The Ni@TiO$_{2-x}$(450) catalyst was prepared via calcination and reduction process of NiTi-LDH precursor, as reported in our previous work.[19] Herein, in order to reveal the real structure of Ni@TiO$_{2-x}$(450) catalyst (avoiding the oxidation of Ni exposed in air), *in situ* HRTEM measurement was carried out in a closed gas cell at atmospheric pressure, which showed lattice fringe with an interplanar distance of 0.203 nm and a dihedral angle of 70° corresponding to the {111} and the {1−11} plane[33] of face-centered cubic (fcc) Ni phase (Figure 1A, a). The interplanar distance of 0.350 nm is attributed to the {101} plane of hexagonal closed-packed (hcp) TiO$_2$ phase. The selected electron diffraction based on the fast Fourier transform (FFT) patterns (Figure 1A, b) demonstrates three types of diffraction patterns, whose radius of diffractions circle is attributed to {111}, {200} plane of Ni phase (fcc) and {101} plane of TiO$_2$ phase (hcp), respectively, further confirming the structure observed in Figure 1A, a. Moreover, *ex situ* HAADF-STEM and *ex situ* STEM-EDS measurements were performed to investigate the surface structure of Ni@TiO$_{2-x}$(450) sample (Figure 1A, c−g). Elemental mapping analysis based on HAADF-STEM-EDS exhibits a disordered and nonuniform distribution of Ti and O on the surface of Ni particles (Figure 1A, d−g). The line scan spectrum of *ex situ* STEM-EDS was obtained over one individual Ni nanoparticle, which shows a similar Gaussian distribution of O and Ti (Figure S1). This demonstrates that Ni nanoparticles are partially overlaid by TiO$_{2-x}$ coating.

In situ electronic energy-loss spectroscopy (EELS) measurements (Figure 1B) were carried out to further confirm the encapsulation structure and to identify the electronic state focus at various locations (e.g., surface Ni metal, interface, TiO$_{2-x}$ support). As shown in Figure 1B, Ti *L*-edge, O *K*-edge and Ni *L*-edge spectra were collected on three selected locations (Figure 1B, a and b: Spot A, B and C), respectively. Only Ni *L*-edge spectra are observed at Spot A, indicating the location of metal Ni species. Spot B is composed of both Ti *L*-edge and O *K*-edge spectra, which represents the TiO$_{2-x}$ support. In the case of Spot C, all of Ti *L*-edge, O *K*-edge and Ni *L*-edge spectra are identified, indicating the interfacial site between metal and support. The results above verify that the Ni nanoparticles were encapsulated partially by disordered TiO$_{2-x}$ overlayer,[4] in agreement with the HAADF-STEM and STEM-EDS measurements. Furthermore, the Ti *L*-edge spectra[34] and O *K*-edge spectra collected at Spot C (interface) and Spot B (support) show similar peak type, indicating that the chemical state of TiO$_{2-x}$ overlayer located at the interface is close to that of TiO$_{2-x}$ support.

3.2. Studies on Electronic Metal−Support Interactions over Ni@TiO$_{2-x}$(450) Sample. *In situ* X-ray photoelectron spectroscopy (XPS) combined with *ex situ* X-ray absorption spectroscopy (XAS) of Ni *L*$_{II,III}$-edge and Ti *L*$_{II,III}$-edge were performed to explore the electronic metal−support interactions (EMSI). *In situ* XPS Ni 2p and Ti 2p spectra
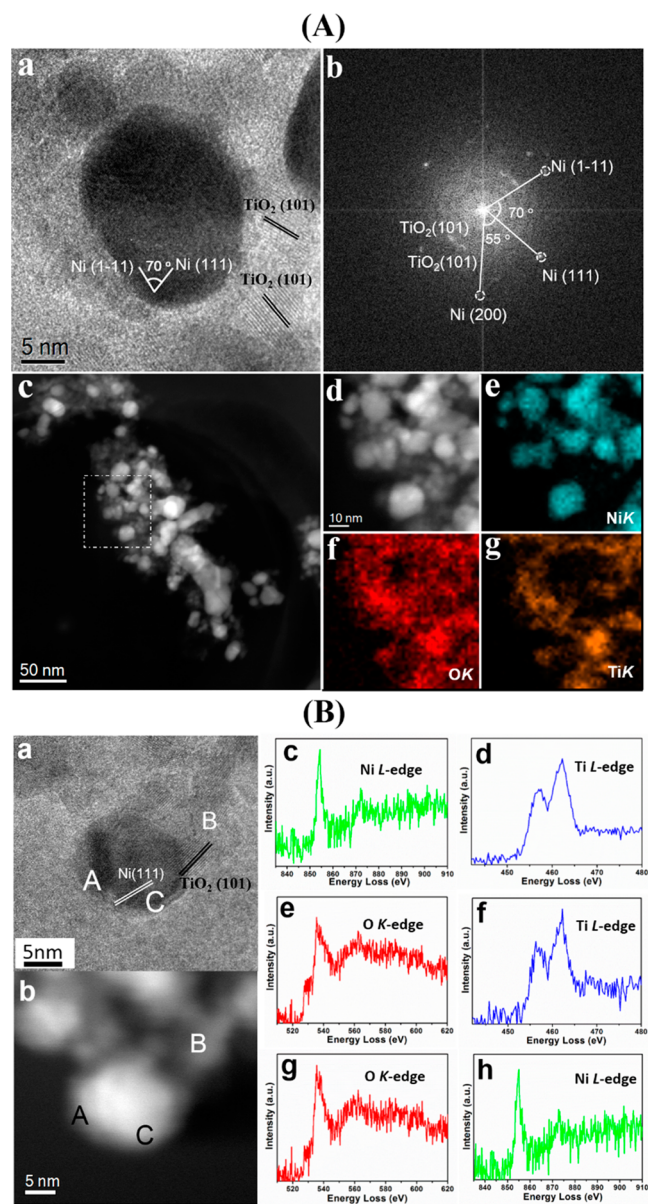
Figure 1. (A): (a,b) *In situ* HRTEM image of the Ni@TiO$_{2-x}$(450) sample. (c) *Ex situ* HAADF-STEM image of the Ni@TiO$_{2-x}$(450) sample. (d) The white dashed line box area in panel c with element EDS mapping of (e) Ni, (f) O and (g) Ti, respectively. (B): (a) *In situ* HRTEM images for the Ni@TiO$_{2-x}$(450) sample, after reduction at 450 °C in 10% H$_2$ atmosphere for 1 h and cooled to room temperature. (b) *In situ* HAADF-STEM images of panel a. *In situ* electron energy-loss spectroscopy (EELS) collected at Spot A, B, C in panel b, respectively, with a single spot size of ~1 nm. (c) Ni *L*-edge spectra collected at Spot A. (d) Ti *L*-edge spectra and (e) O *K*-edge spectra collected at Spot B. (f) Ti *L*-edge spectra, (g) O *K*-edge spectra and (h) Ni *L*-edge spectra collected at Spot C.

(Figure S2a,b) were collected after the reduction of Ni@TiO$_{2-x}$(450) at 450 °C for 1 h (10% H$_2$ atmosphere), and were deconvoluted by Gaussian peak fitting method. The peaks at ~852.4 and ~853.7 eV are attributed to Ni^0 and Ni^{2+} species, respectively.[35] Notably, one special peak at ~851.7 eV is observed, which is attributed to Ni$^{\delta-}$ (electron-enriched Ni species). *Ex situ* XAS spectra of Ni *L*$_{II,III}$-edge (Figure S2c) show that the absorption edge shifts to the lower energy compared with the Ni foil, further confirming the existence of
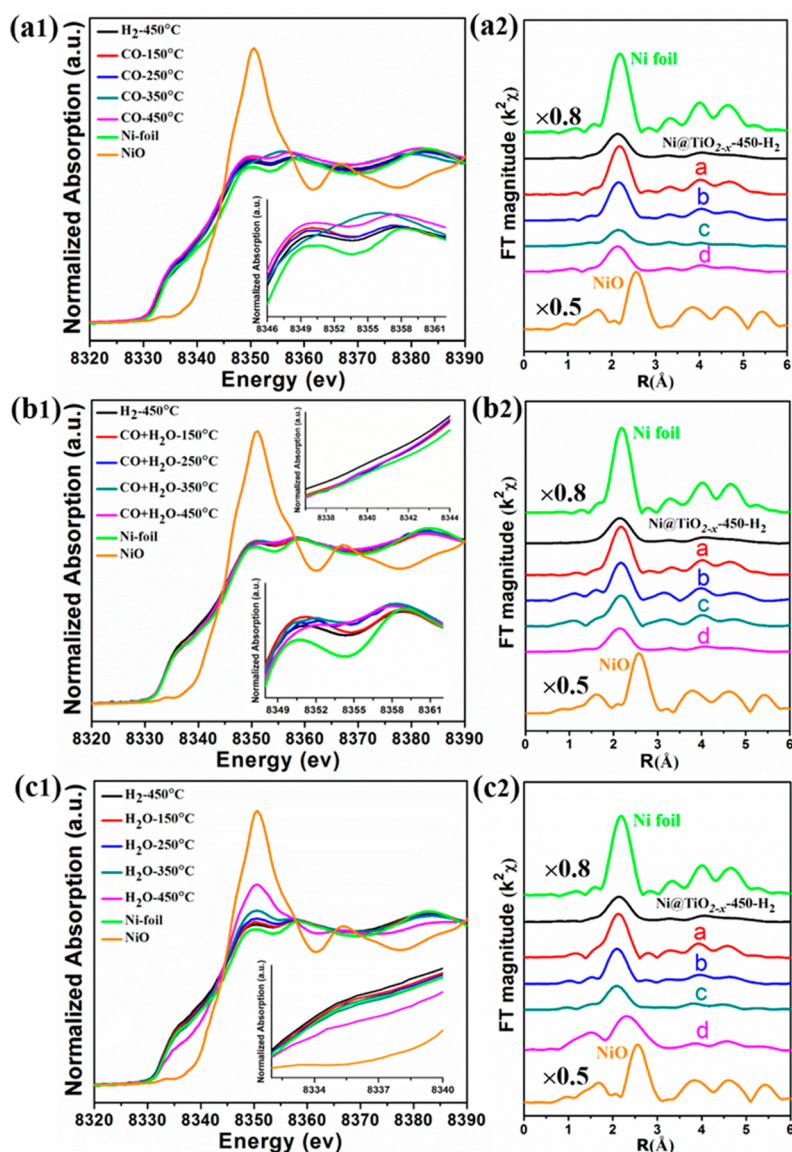
Figure 2. Normalized Ni K-edge XANES spectra for Ni@TiO$_{2-x}$(450) catalyst in (a1) CO atmosphere, (b1) CO+H$_2$O atmosphere (*operando* conditions), (c1) H$_2$O atmosphere at 150, 250, 350 and 450 °C, respectively. Ni foil and NiO reference sample: room temperature. Fourier-transform Ni K-edge EXAFS spectra for Ni@TiO$_{2-x}$(450) catalyst in (a2) CO atmosphere, (b2) CO+H$_2$O atmosphere (*operando* conditions), (c2) H$_2$O atmosphere at (a) 150 °C, (b) 250 °C, (c) 350 °C and (d) 450 °C, respectively.

Ni$^{\delta-}$ species. In the case of *in situ* XPS Ti 2p spectra (Figure S2b), abundant Ti^{3+} species were observed via a deconvoluted Ti 2p$_{3/2}$ peak at ~457.5 eV.[36] Furthermore, the formation of electron-enriched Ni$^{\delta-}$ and five-coordinated Ti^{3+} species (associated with oxygen vacancies) in the Ni@TiO$_{2-x}$(450) sample has also been observed by *in situ* XANES spectra and *in situ* DRIFTS spectra in our previous work.[19] A combination study of *in situ* XPS, *in situ* EELS spectra (Figure 1B), and *ex situ* XAS spectra of Ti $L_{II,III}$-edge (Figure S2d) in this work demonstrates that the TiO$_{2-x}$ overlayer modified on the surface of Ni particles promotes the electronic migration from TiO$_{2-x}$ support to Ni atoms located at the interface, accompanied by the formation of abundant interfacial sites (Ni$^{\delta-}$−O$_v$−Ti^{3+}).

In our previous work, the Ni@TiO$_{2-x}$(450) catalyst showed excellent catalytic activity at 350 °C for WGS reaction, and the Ni$^{\delta-}$−O$_v$−Ti^{3+} interfacial site has been proved as the active

site.[19] In this work, *in situ/operando* EXAFS, *in situ* DRIFTS combined with TPSR measurements were performed to acquire direct evidence of Ni$^{\delta-}$−O$_v$−Ti^{3+} interfacial site in accelerating WGS reaction. By virtue of monitoring the electronic state and structural evolution of interfacial site under *in situ* and *operando* conditions, a new mechanism on interfacial synergistic catalysis toward WGS reaction was proposed.

3.3. *In Situ/Operando* Insight into the CO Adsorbate-Induced Surface Reconstruction. It is generally accepted that chemisorption and activation of CO molecule occur on the surface of metal during the WGS reaction.[11,14] *In situ/operando* EXAFS were performed to give the structural information in detail and the corresponding change of the electronic structure, coordination environment and bond distance in pristine CO atmosphere and under reaction conditions, respectively. The normalized Ni K-edge XANES

spectra of Ni@TiO$_{2-x}$(450) catalyst (Figure 2a1) were obtained in H$_2$/He (1:19, v/v) atmosphere at 450 °C for 30 min (prereduction), subsequently flushed with He for 30 min, and exposed in CO/He (1:19, v/v) atmosphere at 150, 250, 350 and 450 °C, respectively. Obviously, the strength of white line for Ni@TiO$_{2-x}$(450) sample is slightly higher than of Ni foil but rather close to Ni foil after reduction at 450 °C, indicating the predominant Ni^0 species in the catalyst. The absorption edge shifts slightly to lower photon energy relative to Ni foil, owing to the electron transfer from TiO$_{2-x}$ support to Ni atom at the interface via a strong EMSI. Moreover, the white line increases slightly within the temperature from 150 to 250 °C under CO atmosphere conditions, but the absorption edge is very similar to that in H$_2$ atmosphere, probably due to the electron donation of Ni atom (i.e., d-electrons of Ni atom into the 2π* antibonding orbital of CO).[37] Interestingly, as the temperature increases to 350 °C, the white line decreases sharply and a new peak at ~8355 eV appears, which suggests a CO adsorbate-induced surface reconstruction. With the temperature rising to 450 °C, the white line shows a noticeable increment but the absorption edge shifts to low photon energy, indicating a surface charge polarization resulting from the EMSI. Previous study has reported a similar phenomenon, in which the charge polarization at the interface induced by electronic perturbation significantly enhances its chemical activity.[24,38] This requires modification of the electronic properties at metal surface and the formation of oxygen vacancies defects located at the interface.

In situ DRIFTS measurements were carried out to further reveal the CO adsorbate-induced surface reconstruction (Figure S3). Two IR bands are observed at ~2065 and ~2035 cm^{-1} at 25 °C, which are attributed to linear adsorption of CO molecule on the surface of low-coordinated Ni site and saturation-coordinated Ni site,[19] respectively. The IR band located at ~1870 cm^{-1} is assigned to CO bridge adsorption on the electron-enriched Ni$^{\delta-}$ located at the interface; while the one at ~1945 cm^{-1} is attributed to CO bridge adsorption on the interfacial Ni$^{\delta-}$ site or bridge Ni sites of Ni particles. In order to further confirm this conclusion, DFT calculations were carried out to explore the Bader charges on Ni(111) surface and Ni(111)@TiO$_{2-x}$(101) interface before and after CO adsorption, respectively. As shown in Table S1, upon CO adsorption, the Ni atoms (Ni$_1$ site and Ni$_2$ site in Figure S4) located at the Ni(111)@TiO$_{2-x}$ interface transfer more electrons to adsorbed CO molecule than those on the surface of Ni(111), increasing the back-donation of Ni d-electrons into the 2π* antibonding orbital of CO, which explains the lower CO streching frequency at Ni(111)@TiO$_{2-x}$ interface. Interestingly, as the temperature increases to 150 °C, two linear adsorption bands disappear, indicating the desorption of CO molecule from the surface of Ni particles. Meanwhile, the IR band of CO bridge adsorption shifts to the higher frequency (i.e., blue shift) with the increment of temperature. As shown in Figure 2a1 (inset: red line), upon exposing the fresh Ni@TiO$_{2-x}$ catalyst to CO atmosphere (5% CO, He balance), the white line of XANES spectra at Ni K-edge increases slightly, in accordance with the blue shift of CO IR band. Furthermore, as shown in Figure S5, the intensity of CO adsorption band on the surface of Ni particles in 20% Ni/Al$_2$O$_3$ catalyst substantially decreases with the increase of temperature and no IR band is observed after flushing with He when the temperature exceeds 50 °C. However, the intensity of CO band on Ni@TiO$_{2-x}$ catalyst decreases slightly from room

temperature to 150 °C (Figure S3). This indicates that the CO adsorption on the interfacial sites (Ni$^{\delta-}$) is less influenced by temperature. Based on the results mentioned above, the new band at ~2020 cm^{-1} is related to the CO-adsorption induced surface reconstruction, rather than the desorption of CO molecule on bridge sites at high temperature. Because of the disappearance of IR band at ~1945 cm^{-1} accompanied by the formation of new band at ~2020 cm^{-1}, we attribute this change to the transformation from bridge adsorption to linear adsorption at the interface Ni$^{\delta-}$. Moreover, as the temperature rises to 350 °C, both the new linear adsorption and bridge adsorption shift to high frequency (from ~2020 and ~1870 cm^{-1} to ~2036 and ~1907 cm^{-1}, respectively), indicating a decreased electron d-π back-donation from Ni$^{\delta-}$ to CO. More detailed investigations on CO adsorbate-induced surface reconstruction will be carried out in our future work.

The FT k^2-weighted Ni K-edge EXAFS spectra (i.e., the R-space plot) for Ni@TiO$_{2-x}$(450) catalyst were obtained to further explore the CO adsorbate-induced surface reconstruction. As shown in Figure 2a2 and Figures S6–S8, the peaks in curve-fitting within the R range of 1–3 Å were attributed to the first shell of NiO phase, the first shell of metallic Ni and the second shell of NiO phase, respectively. The fitting results including Debye–Waller factor, bond distance, and coordination number are listed in Table S2. Obviously, the bond distance of Ni–Ni remains constant with the increment of temperature in the CO atmosphere. The EXAFS spectrum of Ni@TiO$_{2-x}$(450) sample at 350 °C confirms that Ni–O shell (~1.83 Å) and Ni–Ti shell (~2.98 Å) were observed after exposure to CO atmosphere and shows the lowest coordination number and the high Debye–Waller factor, demonstrating a CO adsobate-induced surface reconstruction. In order to exclude the influence of temperature effect, *in situ* EXAFS measurements were performed in He and H$_2$/He (1:19, v/v) atmosphere at 150, 250, 350 and 450 °C, respectively (Figure S9). No obvious change is observed both in the absorption edge and bond distance of Ni@TiO$_{2-x}$(450) catalyst at different temperatures, indicating temperature effect in an inert atmophere shows a neglectable influence on the structure of Ni@TiO$_{2-x}$(450) sample. The results above verify that activated adsorption of CO occurs on the surface of metallic Ni, which induces a surface reconstruction especially at high temperature.

Operando EXAFS was carried out to further explore elaborately the change of electronic state and geometrical structure of Ni@TiO$_{2-x}$(450) catalyst under practical conditions (Figure 2b1 and 2b2). The fitting results including Debye–Waller factor, bond distance and coordination number are listed in Table S3. The nomalized Ni K-edge XANES spectra collected at different temperatures are similar to the fresh catalyst. The white line of metallic Ni shows an irregular change in the studied temperature range: it increases slightly at 150 °C and then decreases at 250 °C; a further enhancement is observed at 350 °C followed by a sharp decrease at 450 °C. Obviously, the *operando* change of white line within 150–450 °C is very different from that in CO atmosphere, which is attributed to the continuously renewed catalyst surface as a result of the reaction between adsorbed CO and H$_2$O molecule. This disordered change of white line is possibly due to the electronic oscillation during reaction. The FT k^2-weighted Ni K-edge EXAFS spectra (i.e., the R-space plot) show a slight decrease in the Ni–Ni coordination number with constant bond distance from 150 to 450 °C (Figure S10 and
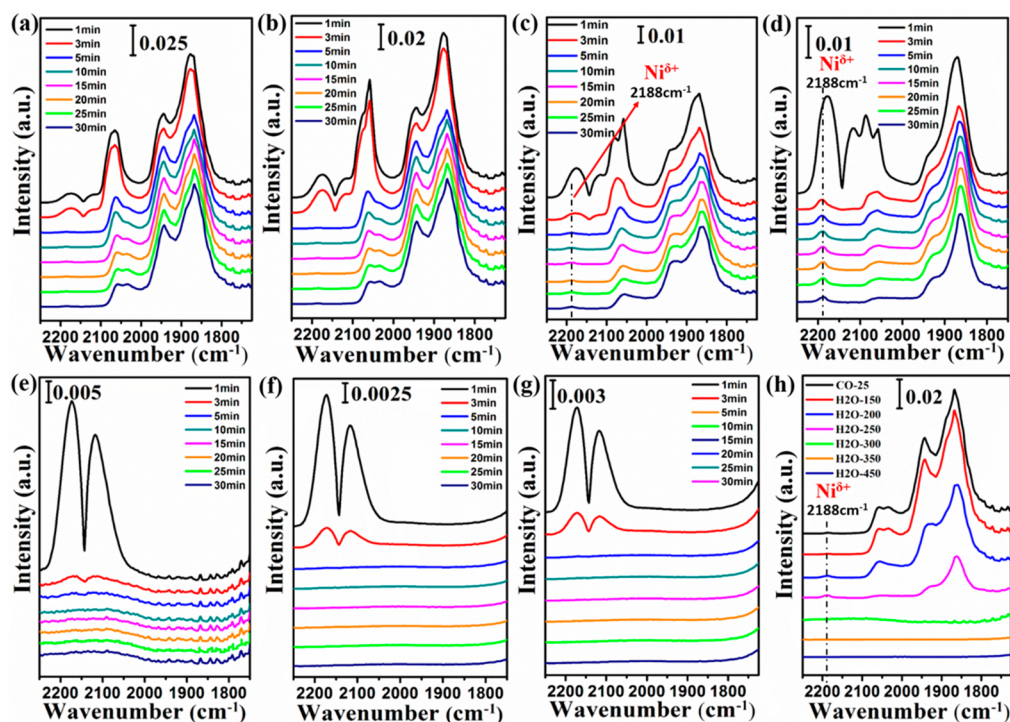
Figure 3. *In situ* DRIFTS spectra of CO chemisorption over Ni@TiO$_{2-x}$(450) catalyst at 25 °C: (a) fresh catalyst after reduction at 450 °C for 30 min followed by He flushing for 30 min; exposing to H$_2$O atmosphere at (b) 150 °C, (c) 200 °C, (d) 250 °C, (e) 300 °C, (f) 350 °C, (g) 450 °C for 30 min followed by He flushing for 30 min. (h) *In situ* DRIFTS spectra of CO chemisorption over Ni@TiO$_{2-x}$(450) catalyst at 25 °C (from top to bottom: without H$_2$O atmosphere at 25 °C and upon exposure to H$_2$O atmosphere at 150, 200, 250, 300, 350 and 450 °C, respectively).

Table S3), which is probably due to the CO adsorption-induced surface construction under *operando* conditions.

3.4. *In Situ* Investigations on H$_2$O Dissociation over Ni@TiO$_{2-x}$(450) Catalyst. It has been commonly recognnized that the activated dissociation of H$_2$O molecule is the rate-determining step in WGS reaction.[7,39] Herein, three kinds of *in situ* characterization techniques were used to give detailed electronic and structural evolution information during H$_2$O dissociation at different temperatures. *In situ* EXAFS spectrum of fresh Ni@TiO$_{2-x}$(450) catalyst (Figure 2c1) shows a slight shift of absorption edge toward low photon energy relative to Ni foil, which is due to the electron transfer from TiO$_{2-x}$ support to Ni atom at the interface. However, upon exposure to H$_2$O atmosphere at 150 °C, the normalized XANES spectrum of Ni K-edge displays a slight enhancement in the white line with a high-energy-shift of absorption edge; moreover, the white line increases gradually and concomitantly the absorption edge shifts progressively toward high photon energy relative to Ni foil from 250 to 450 °C (Figure 2c1). This indicates the electron transfer from Ni species to TiO$_{2-x}$, as a result of the oxidation of metallic Ni at an elevated temperature. The FT k^2-weighted Ni K-edge EXAFS spectra (i.e., the R-space plot) for Ni@TiO$_{2-x}$(450) catalyst were obtained to investigate the H$_2$O dissociation process at different temperatures (Figure 2c2 and Figure S11), and the fitting results are listed in Table S4. Surprisingly, the formation of Ni−O bond attributed to the first shell of NiO phase is detected within the temperature range 250−450 °C, but the bond distance is shorter than NiO crystalline phase. This confirms that the metallic Ni is gradually oxidized to NiO-like phase during the water dissociation (Ni$^{\delta+}$, 0 < δ < 2). In addition, a new peak at ∼3.08 Å is observed at 450 °C (Figure 2c2), which is attributed to the formation of Ni−O−Ti bond

based on the corresponding curve-fitting results, with a longer bond distance relative to the Ni−O−Ni bond (∼2.94 Å) in NiO crystalline phase. In order to further confirm the active site for H$_2$O dissociation, *in situ* EXAFS of powdered Ni as a control sample (particle size: 30−50 nm, Figure S12) was performed to investigate whether pure Ni particles can promote the H$_2$O dissociation. The normalized Ni K-edge XANES spectra of powdered Ni sample do not show obvious change upon exposure in H$_2$O atmosphere within the temperature range from 150 to 450 °C (Figure S13A, curves b−f), with the absence of both Ni−O bond (∼2.09 Å) and Ni−O−Ti bond (∼3.08 Å) in Fourier-transform Ni K-edge EXAFS spectra during the same process (Figure S13B). This verifies that H$_2$O dissociation cannot occur on the surface of pure Ni particles within 150−450 °C. Therefore, the results above demonstrate that H$_2$O molecule undergoes dissociation at the metal−support interface (Ni$^{\delta-}$−O$_v$−Ti^{3+} interfacial sites), accompanied by the oxidation of Ni$^{\delta-}$−O$_v$−Ti^{3+} interfacial site to Ni$^{\delta+}$−O−Ti^{4+} species. With the increment of temperature, the bond distance of Ni−O in the NiO-like phase decreases gradually (Figure 2c2 and Table S4), indicating an enhancement in the oxidation state of Ni$^{\delta+}$. In contrast, the Ni−Ni bond distance increases gradually at an elevated temperature, suggesting an adsorption-induced interfacial reconstruction during the H$_2$O dissociation.

In situ DRIFTS measurements were carried out to further explore the electronic structure of Ni$^{\delta+}$ during H$_2$O dissociation on the surface of Ni@TiO$_{2-x}$(450) sample, by using CO as a probe molecule. For the fresh Ni@TiO$_{2-x}$(450) catalyst (Figure 3a), two bands at 2030 and 2075 cm^{-1} are due to the linear CO adsorption on metallic Ni; and a broad dominant band within 1800−2000 cm^{-1} is ascribed to the bridge CO adsorption[40,41] (probably located at the interface),
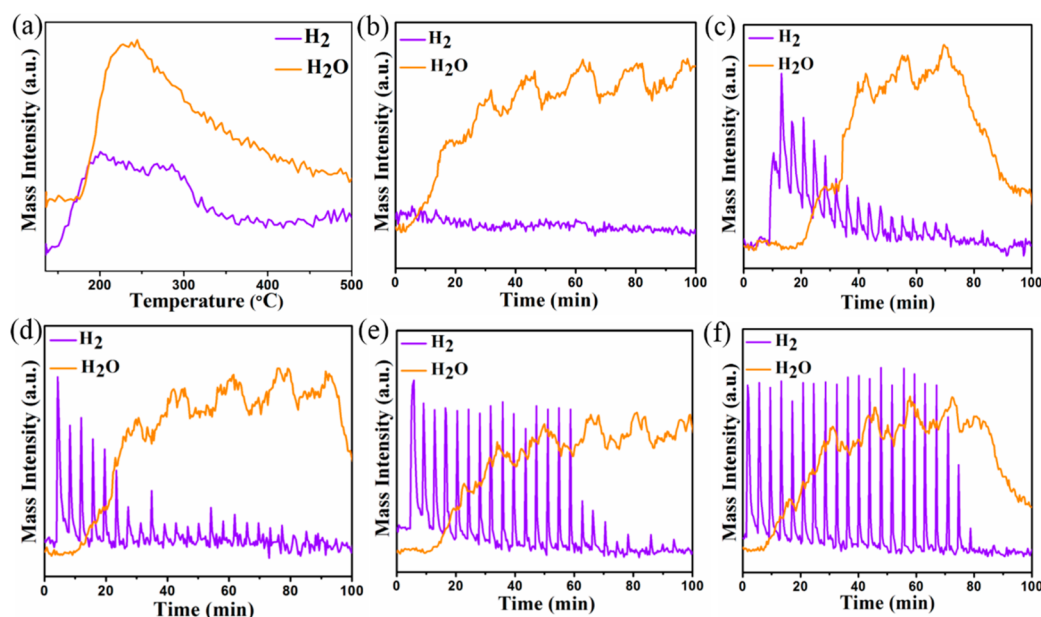
Figure 4. (a) Mass signals of H_2 and H_2O during *in situ* TPD-MASS measurement over Ni@TiO$_{2-x}$(450) catalyst; mass signals of H_2 and H_2O after pulsing water over Ni@TiO$_{2-x}$(450) catalyst at (b) 150 °C, (c) 200 °C, (d) 250 °C, (e) 350 °C and (f) 450 °C, respectively, for 30-time-cycle in 3 min.

indicating that the Ni$^{\delta-}$ species enhances the d-electron back-donation of Ni atom. As the fresh Ni@TiO$_{2-x}$(450) catalyst was exposed to H_2O atmosphere at 150 °C for 30 min (Figure 3b), no obvious change in the CO adsorption bands was found. However, as the temperature increased from 200 to 250 °C (Figure 3c−d), the two main peaks deceased gradually within 1800−2000 cm^{-1} while a new IR band of CO adsorption at 2188 cm^{-1} was observed, which was attributed to Ni$^{\delta+}$ species originating from the oxidation of Ni$^{\delta-}$ by H_2O molecule. This indicates that the valence state of Ni$^{\delta+}$ is between zero valence and divalence (probably monovalence), in accordance with the observation from *in situ* EXAFS. In the temperature range 300−450 °C (Figure 3e−g), no IR band of CO chemisorption can be detected, owing to the oxidation of Ni$^{\delta-}$ to a higher valence, corresponding to the stronger white line and shorter distance of Ni−O bond as revealed by *in situ* XAFS.

In situ TPD-MASS combined with H_2O Pulse-MASS at different temperatures were carried out to explore the temperature dependence and products of H_2O dissociation. First, fresh Ni@TiO$_{2-x}$(450) catalyst was pretreated in water atmosphere[42] at 120 °C for 15 min and subsequently flushed with He for 15 min. Afterward, *in situ* TPD-MASS was performed within the temperature range from 120 to 500 °C[17] with a heating rate of 5 °C min^{-1} as shown in Figure 4a. The generation of H_2 is detected at ~150 °C (Temperature$_{peak}$ = 201 °C), indicating that the dissociation of water molecule to produce hydrogen occurs on the surface of Ni@TiO$_{2-x}$(450) catalyst above 150 °C. Furthermore, H_2O Pulse-MASS measurements were performed at 150, 200, 250, 350 and 450 °C, respectively, to further verify the water dissociation process. As shown in Figure 4b−f, H_2 evolution is not found at 150 °C, but is detected within the temperature range 200−450 °C with increasingly enhanced amount of H_2 production, corresponding to the oxidation of Ni$^{\delta-}$ to Ni$^{\delta+}$ species. Similar phenomenon has been reported previously in the Pt/CeO$_2$ system, in which the cleavage of O−H in water to generate H_2

during water dissociation was observed.[17] The results above demonstrate that the Ni@TiO$_{2-x}$(450) catalyst shows a high performance toward H_2O dissociation to H_2, as a result of strong electronic metal−support interaction (EMSI) between Ni and TiO$_{2-x}$ support. During the water dissociation at an elevated temperature, the interfacial Ni$^{\delta-}$−O$_v$−Ti^{3+} species were oxidized to Ni$^{\delta+}$−O−Ti^{4+} species, which has been revealed by the *in situ* EXAFS and *in situ* DRIFTS spectra.

It is generally accepted that reducible oxide support plays an important role during the water dissociation process in heterogeneous catalytic WGS reaction.[7,15,16] Previous studies demonstrated that dissociative adsorption of H_2O occurs at oxygen vacancies of reducible support to generate active hydroxyl or oxygen species, and the admetals on the surface indirectly accelerate H_2O dissociation through promoting the formation of oxygen vacancies during the reduction of catalysts. In this work, however, *in situ* Ni K-edge XANES spectra, *in situ* DRIFTS combined with *in situ* TPD-MASS measurements definitely substantiate that the interfacial Ni$^{\delta-}$−O$_v$−Ti^{3+} species take part in the water dissociation: electron-enriched species (Ni$^{\delta-}$) located at the interface is oxidized to Ni$^{\delta+}$ at above 150 °C accompanied by the formation of Ni$^{\delta+}$−O−Ti^{4+} species, and water molecule is reduced to hydrogen. Based on the results above, the strong EMSI present in the Ni@TiO$_{2-x}$(450) catalyst substantiallly facilitates H_2O dissociation, i.e., the electron located at the interface tremendously accelerates the cleavage of O−H bond in water to produce hydrogen.

3.5. *In Situ* Time-Resolved Studies on the Whole Catalytic Process toward WGS Reaction. *In situ* time-resolved DRIFTS spectra (Figure 5) were carried out to study the catalytic performance of active site (interfacial site) toward WGS reaction. The CO adsorption spectra on the surface of Ni@TiO$_{2-x}$(450) catalyst were recorded within the temperature range 30−200 °C (Figure S14a). The CO bridge adsorption at 1850−1900 cm^{-1} decreased gradually with the increase of temperature, and the linear adsorption at ~2030
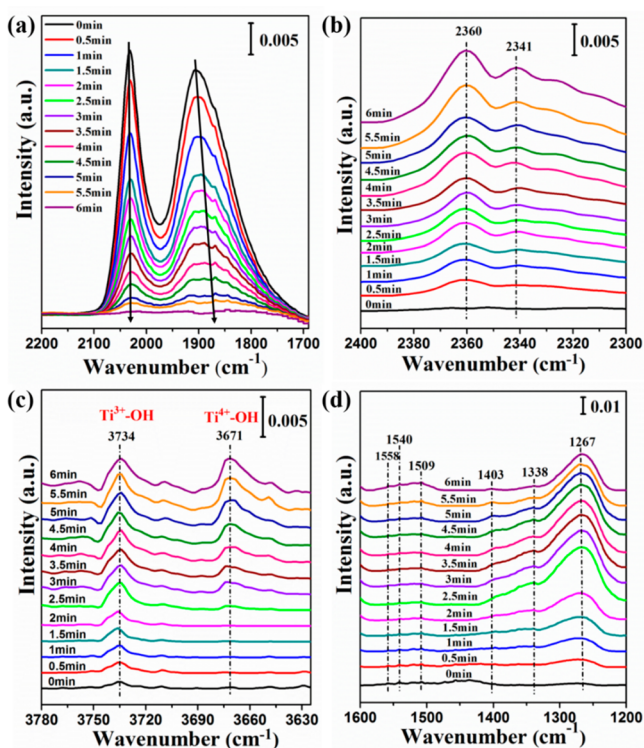
Figure 5. *In situ* time-resolved DRIFTS spectra of CO adsorption on Ni@TiO$_{2-x}$(450) catalyst recorded in (a) 2200−1700 cm^{-1}, (b) 2400−2300 cm^{-1}, (c) 3780−3625 cm^{-1} and (d) 1600−1200 cm^{-1} upon exposure to H$_2$O atmosphere at 200 °C as a function of reaction time.

cm^{-1} enhanced progressively, which is due to the CO adsorption-induced surface reconstruction[43,44] accompanied by the interfacial electronic polarization as observed by *in situ* EXAFS. Afterward, the CO adsorption was flushed with He at 200 °C for 30 min, and two main chemisorption bands of CO at ∼2033 and ∼1903 cm^{-1} were observed (Figure S14b). Subsequently, with the introduction of H$_2$O vapor at 200 °C (Figure 5a), the bands of CO (∼2033 and ∼1903 cm^{-1}) decreased gradually; while two new bands at 2341 and 2360 cm^{-1} attributed to adsorbed CO$_2$ molecule[40] were observed (Figure 5b). This demonstrates that the adsorbed CO molecule on Ni site reacts with H$_2$O molecule at 200 °C to produce CO$_2$ molecule. Meanwhile, two new bands at 3734 and 3671 cm^{-1} attributed to the Ti^{3+}−OH and Ti^{4+}−OH[45] are observed in Figure 5c, verifying that O$_v$−Ti^{3+} directly participates in H$_2$O dissociation; and Ti^{3+}−OH and Ti^{4+}−OH serve as active intermediate products to further generate hydrogen. Accordingly, the primary IR band at 1267 cm^{-1} increases gradually after exposure to H$_2$O vapor at 200 °C accompanied by the formation of IR bands at 1540 and 1509 cm^{-1} (Figure 5d), all of which are attributed to the O−C−O stretching mode of carboxylate species (CO$_2$$^{\delta-}$).[46−48] Simultaneously, IR bands at 1558, 1338 and 1403 cm^{-1} come into formation, assigned to bidentate carbonate and bicarbonate-type chemisorbed carbon dioxide species.[49] Moreover, no IR band is observed in the C−H stretching spectral region of HCOO species (3000−2800 cm^{-1}) as shown in Figure S15. The results indicate that WGS reaction mainly undergoes redox mechanism rather than associative mechanism over Ni@TiO$_{2-x}$(450) catalyst. As discussed above, *in situ* EXAFS spectra (Figure 2) combined with *in situ* DRIFTS (Figure 3)

have confirmed that interfacial Ni$^{\delta-}$ species participates in H$_2$O dissociation, accompanied by the oxidation of Ni$^{\delta-}$−O$_v$−Ti^{3+} to Ni$^{\delta+}$−O−Ti^{4+} species. Based on the results above, we directly observe that H$_2$O molecule dissociates at the interfacial site (Ni$^{\delta-}$−O$_v$−Ti^{3+}) with the generation of H$_2$, followed by the reaction between Ni$^{\delta+}$−O−Ti^{4+} species and adsorbed CO molecule to produce CO$_2$. In order to further confirm this issue, *in situ* time-resolved DRIFTS spectra were also carried out upon exposure to H$_2$O at 150 and 350 °C, respectively. As shown in Figures S16 and S17, with the presence of H$_2$O vapor at 150 °C for 3 h, the IR band of CO (∼2020 and ∼1893 cm^{-1}) decreased very slightly without the observation of CO$_2$ band, indicating the oxidation of CO molecule cannot occur at 150 °C. Furthermore, as the temperature rose to 350 °C (Figures S18 and S19), the bands of adsorbed CO molecule decreased quickly with the appearance of CO$_2$ bands (at 3734 and 3671 cm^{-1}) within 120 s, which substantiated that CO undergoes reaction with dissociated H$_2$O molecule through WGS reaction at an elevated temperature (above 150 °C).

DFT calculations were performed to further explore the optimal active site of WGS reaction over Ni@TiO$_{2-x}$(450) catalyst. Recently, a multiscale (DFT/microkinetic) modeling approach combined with experimental studies was carried out by Foppa et al., which verified that the metal/support interface of Ni/Al$_2$O$_3$ catalyst provides active sites for WGS reaction.[50] For a comparison study, we investigated the process of H$_2$O dissociation over the Ni(111) surface, Ni(111)@TiO$_{2-x}$(101) interface and TiO$_{2-x}$(101) surface (located at the oxygen vacancy), respectively (Figure 6). Previous studies have suggested that water dissociation is the rate-limiting step of WGS reaction,[51] as H$_2$O reduction is more thermodynamically unfavorable than CO oxidation. We accept this viewpoint here, although there might be some assumptions in this case. As shown in Figure 6d, the activation barrier values of H$_2$O dissociation on Ni(111) surface[24,52] and TiO$_{2-x}$(101) surface[27] (H$_2$O is adsorbed on the five-coordinated Ti) are calculated to be ∼0.87 and ∼0.42 eV, respectively, indicating an unfavorable kinetics in the former case and a facile H$_2$O dissociation in the latter case. In the TiO$_{2-x}$(101) system, although CO molecule is prone to reaction with the surface hydroxyls (from H$_2$O dissociation) to produce active intermediate species (e.g., COOH, HCOO, or HCO$_3^-$ species), the transformation of intermediate species to CO$_2$ and H$_2$ is rather difficult owing to a high activation energy barrier reported by previous work.[53] Therefore, a reducible oxide support (especially for TiO$_2$, CeO$_2$) itself only shows a poor activity toward WGS reaction.[12,53] In the case of Ni(111)@TiO$_{2-x}$(101) interface[38,54] system (Figure 6b), the E_a value of H$_2$O dissociation further decreases to as low as ∼0.35 eV, which indicates the most favorable process in comparison with Ni(111) surface and TiO$_{2-x}$(101) surface. Both theoretical calculation studies and experimental investigations substantiate that the metal−support interfacial site of Ni@TiO$_{2-x}$(450) catalyst significantly accelerates the H$_2$O dissociation, which serves as the intrinsic active site toward WGS reaction. The concept also holds for Co@TiO$_{2-x}$, Fe@TiO$_{2-x}$ and Cu@TiO$_{2-x}$ catalyst system, which will be elaborately investigated and reported in our future work.

3.6. Reaction Mechanism of Water−Gas Shift Reaction over Ni@TiO$_{2-x}$(450) Catalyst. The temperature-programed surface reaction (TPSR) measurements[42] combined with cycle tests of CO and H$_2$O Pulse-MASS were

Figure 6. Optimized structures for various steps of water dissociation over: (a) Ni(111) surface, (b) Ni(111)@TiO$_{2-x}$(101) interface, (c) TiO$_{2-x}$(101) surface. Ni, O, Ti and H atom are represented as blue, red, gray and white sphere, respectively. (d) Activation barrier of water dissociation over Ni(111) surface, Ni(111)@TiO$_{2-x}$(101) interface and TiO$_{2-x}$(101) surface (located at the oxygen vacancy).

carried out to study the formation of H$_2$ and CO$_2$ at different temperatures over Ni@TiO$_{2-x}$(450) catalyst. As shown in Figure S20, the CO+H$_2$O TPSR were recorded within 125–400 °C at a heating rate of 5 °C/min. Obviously, the initial temperature of H$_2$ evolution is ~175 °C, which is lower than that of CO$_2$ evolution (~200 °C). Combined with the results of *in situ* DRIFTS and *in situ/operando* EXAFS, it is concluded that H$_2$O molecule preferentially dissociates at the interfacial site (Ni$^{\delta-}$–O$_v$–Ti^{3+}) to produce H$_2$ followed by subsequent oxidation of CO to CO$_2$. In order to further investigate the redox process, the cycle pulse of H$_2$O vapor and CO atmosphere experiments (Figure S21) were performed with an interval of 5 min at 200, 250, 350 and 450 °C, respectively. After pulsing H$_2$O vapor into the reactor, H$_2$ formation was detected with enhanced production at elevated temperature. Subsequently, cycle pulse of CO atmosphere was introduced into the reactor, and CO$_2$ formation was observed immediately. In addition, the amount of H$_2$ production in the CO preadsorbed system is much larger than that without CO preadsorbed system, indicating that the adsorption of CO on the surface of Ni facilitates the dissociation of H$_2$O molecule, in accordance with the observation by *in situ* time-resolved DRIFTS. Based on the experimental and calculation studies above, a new insight into interfacial synergistic catalysis

involving redox mechanism is determined: (i) H$_2$O molecule undergoes dissociation at the interfacial site (Ni$^{\delta-}$–O$_v$–Ti^{3+}) to generate H$_2$ accompanied by the formation of active oxygen species (Ni$^{\delta+}$–O–Ti^{4+} species); (ii) active oxygen species react with CO molecule chemically adsorbed on the interfacial Ni$^{\delta+}$ site to produce CO$_2$, with concomitant reduction of Ni$^{\delta+}$–O–Ti^{4+} species to Ni$^{\delta-}$–O$_v$–Ti^{3+}. The whole reaction mechanism over Ni@TiO$_{2-x}$(450) catalyst is described by eqs 1–5 and illustrated in Figure 7.

$$\text{Ni}^{\delta-}-\text{O}_v-\text{Ti}^{3+} \xrightarrow{\text{H}_2\text{O}} \text{Ni}^{\delta+}-\text{OH}-\text{Ti}^{3+} + \text{H}_{ads} \tag{1}$$

$$\text{Ni}^{\delta+}-\text{OH}-\text{Ti}^{3+} \rightarrow \text{Ni}^{\delta+}-\text{O}-\text{Ti}^{4+} + \text{H}_{ads} \tag{2}$$

$$\text{H}_{ads} + \text{H}_{ads} \rightarrow \text{H}_2 \tag{3}$$

$$\text{Ni}^{\delta+}-\text{O}-\text{Ti}^{4+} \xrightarrow{\text{CO}} \text{Ni}-\text{CO}_2{}^{\delta-} + \text{O}_v + \text{Ti}^{3+} \tag{4}$$

$$\text{Ni}-\text{CO}_2{}^{\delta-} \rightarrow \text{Ni}^{\delta-} + \text{CO}_2 \tag{5}$$
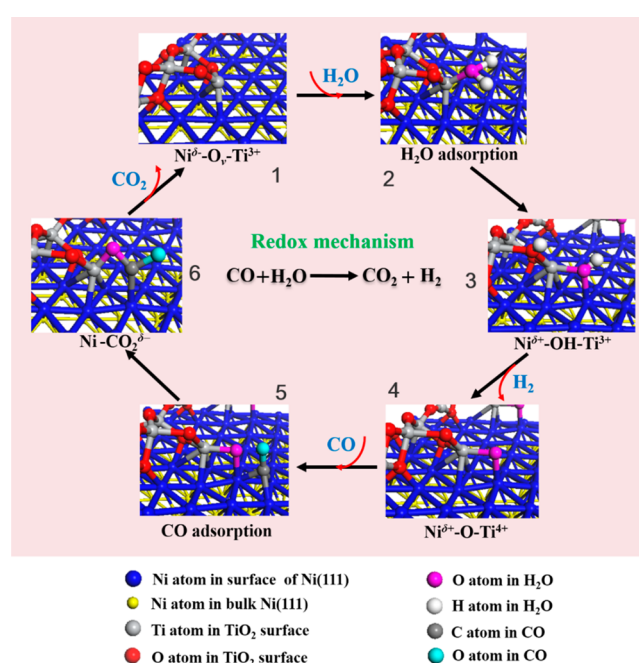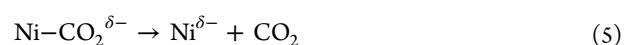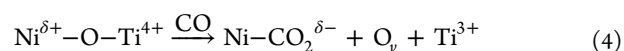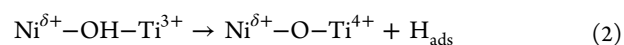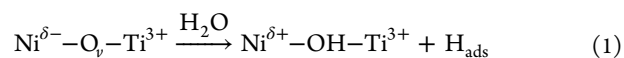
Figure 7. Schematic diagram of WGS reaction over Ni@TiO$_{2-x}$ catalyst based on a redox mechanism.

4. CONCLUSIONS

In summary, the interfacial structure (Ni$^{\delta-}$–O$_v$–Ti^{3+}) derived from strong EMSI between metallic Ni and TiO$_{2-x}$ support was clearly identified. The electron located at the interface accelerates the cleavage of O–H bond in water, and the interfacial metal (Ni$^{\delta-}$) plays a direct role in water dissociation with an activation energy of ~0.35 eV. Both experimental studies and theoretical calculations substantiate that the Ni$^{\delta-}$–O$_v$–Ti^{3+} species (interfacial sites) provide the active center for WGS reaction. A detailed redox mechanism of WGS reaction involving interfacial synergistic catalysis over Ni@TiO$_{2-x}$ catalyst was demonstrated. This work provides a new perspective on intrinsic active sites structure and contributes to the design of high performance heterogeneous catalysts.

ASSOCIATED CONTENT

Ⓢ Supporting Information

The Supporting Information is available free of charge on the ACS Publications website at DOI: 10.1021/jacs.8b03117.

Detailed information on characterizations; additional experimental data (PDF)

AUTHOR INFORMATION

Corresponding Authors
*wangbin.bjhy@sinopec.com
*bszhang@imr.ac.cn
*dma@pku.edu.cn
*weimin@mail.buct.edu.cn
ORCID Ⓞ
Bingsen Zhang: 0000-0002-2607-2999
Ding Ma: 0000-0002-3341-2998
Notes
The authors declare no competing financial interest.

ACKNOWLEDGMENTS

REFERENCES

(1) Graciani, J.; Mudiyanselage, K.; Xu, F.; Baber, A. E.; Evans, J.; Senanayake, S. D.; Stacchiola, D. J.; Liu, P.; Hrbek, J.; Sanz, J. F.; Rodriguez, J. A. *Science* **2014**, *345*, 546.

(2) Fu, Q.; Li, W. X.; Yao, Y.; Liu, H.; Su, H. Y.; Ma, D.; Gu, X. K.; Chen, L.; Wang, Z.; Zhang, H.; Wang, B.; Bao, X. *Science* **2010**, *328*, 1141.

(3) Cargnello, M.; Doan-Nguyen, V. V.; Gordon, T. R.; Diaz, R. E.; Stach, E. A.; Gorte, R. J.; Fornasiero, P.; Murray, C. B. *Science* **2013**, *341*, 771.

(4) Tang, H.; Su, Y.; Zhang, B.; Lee, A. F.; Isaacs, M. A.; Wilson, K.; Li, L.; Ren, Y.; Huang, J.; Haruta, M.; Qiao, B.; Liu, X.; Jin, C.; Su, D.; Wang, J.; Zhang, T. *Sci. Adv.* **2017**, *3*, No. e1700231.

(5) Zhai, Y.; Pierre, D.; Si, R.; Deng, W.; Ferrin, P.; Nilekar, A. U.; Peng, G.; Herron, J. A.; Bell, D. C.; Saltsburg, H.; Mavrikakis, M.; Flytzani-Stephanopoulos, M. *Science* **2010**, *329*, 1633.

(6) Yao, S.; Zhang, X.; Zhou, W.; Gao, R.; Xu, W.; Ye, Y.; Lin, L.; Wen, X.; Liu, P.; Chen, B.; Crumlin, E.; Guo, J.; Zuo, Z.; Li, W.; Xie, J.; Lu, L.; Kiely, C. J.; Gu, L.; Shi, C.; Rodriguez, J. A.; Ma, D. *Science* **2017**, *357*, 389.

(7) Shekhar, M.; Wang, J.; Lee, W. S.; Williams, W. D.; Kim, S. M.; Stach, E. A.; Miller, J. T.; Delgass, W. N.; Ribeiro, F. H. *J. Am. Chem. Soc.* **2012**, *134*, 4700.

(8) Yang, M.; Li, S.; Wang, Y.; Herron, J. A.; Xu, Y.; Allard, L. F.; Lee, S.; Huang, J.; Mavrikakis, M.; Flytzani-Stephanopoulos, M. *Science* **2014**, *346*, 1498.

(9) Ding, K.; Gulec, A.; Johnson, A. M.; Schweitzer, N. M.; Stucky, G. D.; Marks, L. D.; Stair, P. C. *Science* **2015**, *350*, 189.

(10) Fu, Q.; Saltsburg, H.; Flytzani-Stephanopoulos, M. *Science* **2003**, *301*, 935.

(11) Rodriguez, J. A.; Ma, S.; Liu, P.; Hrbek, J.; Evans, J.; Perez, M. *Science* **2007**, *318*, 1757.

(12) Huang, X.; Beck, M. J. *ACS Catal.* **2015**, *5*, 6362.

(13) Rodriguez, J. A.; Graciani, J.; Evans, J.; Park, J. B.; Yang, F.; Stacchiola, D.; Senanayake, S. D.; Ma, S.; Perez, M.; Liu, P.; Sanz, J. F.; Hrbek, J. *Angew. Chem., Int. Ed.* **2009**, *48*, 8047.

(14) Mudiyanselage, K.; Senanayake, S. D.; Feria, L.; Kundu, S.; Baber, A. E.; Graciani, J.; Vidal, A. B.; Agnoli, S.; Evans, J.; Chang, R.; Axnanda, S.; Liu, Z.; Sanz, J. F.; Liu, P.; Rodriguez, J. A.; Stacchiola, D. J. *Angew. Chem., Int. Ed.* **2013**, *52*, 5101.

(15) Zhang, S.; Shan, J. J.; Zhu, Y.; Frenkel, A. I.; Patlolla, A.; Huang, W.; Yoon, S. J.; Wang, L.; Yoshida, H.; Takeda, S.; Tao, F. F. *J. Am. Chem. Soc.* **2013**, *135*, 8283.

(16) Lin, J.; Wang, A.; Qiao, B.; Liu, X.; Yang, X.; Wang, X.; Liang, J.; Li, J.; Liu, J.; Zhang, T. *J. Am. Chem. Soc.* **2013**, *135*, 15314.

(17) Bruix, A.; Rodriguez, J. A.; Ramirez, P. J.; Senanayake, S. D.; Evans, J.; Park, J. B.; Stacchiola, D.; Liu, P.; Hrbek, J.; Illas, F. *J. Am. Chem. Soc.* **2012**, *134*, 8968.

(18) Campbell, C. T. *Nat. Chem.* **2012**, *4*, 597.

(19) Xu, M.; He, S.; Chen, H.; Cui, G.; Zheng, L.; Wang, B.; Wei, M. *ACS Catal.* **2017**, *7*, 7600.

(20) Yeung, C. M. Y.; Meunier, F.; Burch, R.; Thompsett, D.; Tsang, S. C. *J. Phys. Chem. B* **2006**, *110*, 8540.

(21) Montini, T.; Condò, A. M.; Hickey, N.; Lovey, F. C.; De Rogatis, L.; Fornasiero, P.; Graziani, M. *Appl. Catal., B* **2007**, *73*, 84.

(22) Rogatis, L. D.; Vesselli, E.; Baraldi, A.; Casula, M. F.; Montini, T.; Comelli, G.; Graziani, M.; Fornasiero, P. *J. Phys. Chem. C* **2009**, *113*, 18069.

(23) Liao, F.; Zeng, Z.; Eley, C.; Lu, Q.; Hong, X.; Tsang, S. C. E. *Angew. Chem., Int. Ed.* **2012**, *51*, 5832.

(24) Carrasco, J.; Lopez-Duran, D.; Liu, Z.; Duchon, T.; Evans, J.; Senanayake, S. D.; Crumlin, E. J.; Matolin, V.; Rodriguez, J. A.; Ganduglia-Pirovano, M. V. *Angew. Chem., Int. Ed.* **2015**, *54*, 3917.

(25) Mohsenzadeh, A.; Bolton, K.; Richards, T. *Surf. Sci.* **2014**, *627*, 1.

(26) Herman, G. S.; Dohnálek, Z.; Ruzycki, N.; Diebold, U. *J. Phys. Chem. B* **2003**, *107*, 2788.

(27) Tilocca, A.; Selloni, A. *J. Chem. Phys.* **2003**, *119*, 7445.

(28) Perdew, J. P.; Burke, K.; Ernzerhof, M. *Phys. Rev. Lett.* **1996**, *77*, 3865.

(29) Perdew, J. P.; Burke, K.; Wang, Y. *Phys. Rev. B: Condens. Matter Mater. Phys.* **1996**, *54*, 16533.

(30) Chen, H. Y. T.; Tosoni, S.; Pacchioni, G. *ACS Catal.* **2015**, *5*, 5486.

(31) Henkelman, G.; Uberuaga, B. P.; Jonsson, H. *J. Chem. Phys.* **2000**, *113*, 9901.

(32) Skúlason, E.; Tripkovic, V.; Björketun, M. E.; Gudmundsdóttir, S.; Karlberg, G.; Rossmeisl, J.; Bligaard, T.; Jónsson, H.; Nørskov, J. K. *J. Phys. Chem. C* **2010**, *114*, 22374.

(33) Liu, J.; Li, C.; Wang, F.; He, S.; Chen, H.; Zhao, Y.; Wei, M.; Evans, D. G.; Duan, X. *Catal. Sci. Technol.* **2013**, *3*, 2627.

(34) Park, H.; Kwon, J.; Choi, H.; Song, T.; Paik, U. *Sci. Adv.* **2017**, *3*, No. e1700509.

(35) Wang, C.; Zhai, P.; Zhang, Z.; Zhou, Y.; Zhang, J.; Zhang, H.; Shi, Z.; Han, R. P. S.; Huang, F.; Ma, D. *J. Catal.* **2016**, *334*, 42.

(36) Melaet, G.; Ralston, W. T.; Li, C. S.; Alayoglu, S.; An, K.; Musselwhite, N.; Kalkan, B.; Somorjai, G. A. *J. Am. Chem. Soc.* **2014**, *136*, 2260.

(37) Roiaz, M.; Monachino, E.; Dri, C.; Greiner, M.; Knop-Gericke, A.; Schlogl, R.; Comelli, G.; Vesselli, E. *J. Am. Chem. Soc.* **2016**, *138*, 4146.

(38) Wang, Y. G.; Yoon, Y.; Glezakou, V. A.; Li, J.; Rousseau, R. *J. Am. Chem. Soc.* **2013**, *135*, 10673.

(39) Rodriguez, J. A.; Liu, P.; Hrbek, J.; Evans, J.; Perez, M. *Angew. Chem., Int. Ed.* **2007**, *46*, 1329.

(40) Ang, M. L.; Oemar, U.; Kathiraser, Y.; Saw, E. T.; Lew, C. H. K.; Du, Y.; Borgna, A.; Kawi, S. *J. Catal.* **2015**, *329*, 130.

(41) McEntee, M.; Stevanovic, A.; Tang, W.; Neurock, M.; Yates, J. T., Jr *J. Am. Chem. Soc.* **2015**, *137*, 1972.

(42) Zhu, M.; Wachs, I. E. *ACS Catal.* **2016**, *6*, 2827.

(43) Avanesian, T.; Dai, S.; Kale, M. J.; Graham, G. W.; Pan, X.; Christopher, P. *J. Am. Chem. Soc.* **2017**, *139*, 4551.

(44) Raskó, J. *J. Catal.* **2003**, *217*, 478.

(45) Liu, L.; Zhao, C.; Li, Y. *J. Phys. Chem. C* **2012**, *116*, 7904.

(46) Kalamaras, C. M.; Americanou, S.; Efstathiou, A. M. *J. Catal.* **2011**, *279*, 287.

(47) Kalamaras, C. M.; Dionysiou, D. D.; Efstathiou, A. M. *ACS Catal.* **2012**, *2*, 2729.

(48) Vecchietti, J.; Bonivardi, A.; Xu, W.; Stacchiola, D.; Delgado, J. J.; Calatayud, M.; Collins, S. E. *ACS Catal.* **2014**, *4*, 2088.

(49) Kalamaras, C. M.; Panagiotopoulou, P.; Kondarides, D. I.; Efstathiou, A. M. *J. Catal.* **2009**, *264*, 117.

(50) Foppa, L.; Margossian, T.; Kim, S. M.; Müller, C.; Copéret, C.; Larmier, K.; Comas-Vives, A. *J. Am. Chem. Soc.* **2017**, *139*, 17128.

(51) Sun, K.; Kohyama, M.; Tanaka, S.; Takeda, S. *J. Phys. Chem. C* **2017**, *121*, 12178.

(52) Hundt, P. M.; Jiang, B.; van Reijzen, M. E.; Guo, H.; Beck, R. D. *Science* **2014**, *344*, 504.

(53) Toledo-Antonio, J. A.; Capula, S.; Cortes-Jacome, M. A.; Angeles-Chavez, C.; Lopez-Salinas, E.; Ferrat, G.; Navarrete, J.; Escobar, J. *J. Phys. Chem. C* **2007**, *111*, 10799.

(54) Rodriguez, J. A.; Grinter, D. C.; Liu, Z.; Palomino, R. M.; Senanayake, S. D. *Chem. Soc. Rev.* **2017**, *46*, 1824.